UCRL-JC-128201
PREPRINT

Equation of State Measurements of D_2 on Nova

G.W. Collins, L.B. Da Silva, P. Celliers, K.S. Budil,
R. Cauble, D. Gold, M. Foord, R. Stewart, N.C.
Holmes, M. Ross, B.A. Hammel, J.D. Kilkenny,
R.J. Wallace and A. Ng

This paper was prepared for submittal to the
American Physical Society 1997 Conference on
Shock Compression of Condensed Matter
Amherst, MA
July 27-August 1, 1997

July 1997

Lawrence
Livermore
National
Laboratory

This is a preprint of a paper intended for publication in a journal or proceedings. Since changes may be made before publication, this preprint is made available with the understanding that it will not be cited or reproduced without the permission of the author.

DISCLAIMER

This document was prepared as an account of work sponsored by an agency of the United States Government. Neither the United States Government nor the University of California nor any of their employees, makes any warranty, express or implied, or assumes any legal liability or responsibility for the accuracy, completeness, or usefulness of any information, apparatus, product, or process disclosed, or represents that its use would not infringe privately owned rights. Reference herein to any specific commercial product, process, or service by trade name, trademark, manufacturer, or otherwise, does not necessarily constitute or imply its endorsement, recommendation, or favoring by the United States Government or the University of California. The views and opinions of authors expressed herein do not necessarily state or reflect those of the United States Government or the University of California, and shall not be used for advertising or product endorsement purposes.

EQUATION OF STATE MEASUREMENTS OF D_2 ON NOVA

G. W. Collins, L. B. Da Silva, P. Celliers, K. S. Budil, R. Cauble, D. Gold, M. Foord, R. Stewart, N. C. Holmes, M. Ross, B. A. Hammel, J. D. Kilkenny, R. J. Wallace, A. Ng[1]

Lawrence Livermore National Laboratory, Livermore, CA 94550
[1]University of British Columbia, Vancouver B.C.

INTRODUCTION

Condensed molecular hydrogen at low pressure is an insulator with a 15 eV band gap and 4.5 eV molecular binding energy. Theory predicts, even at T=0, both the bandgap and molecular dissociation energy will decrease with increasing pressure, ultimately transforming hydrogen into an atomic metal at ~ 3 Mbar. At pressures between ~ .1 and 3 Mbar, thermal dissociation and ionization can occur at temperatures well below the low pressure limit. How hydrogen transforms from a condensed molecular state into a fully ionized dense plasma is of fundamental interest and has a profound impact on the equation of state (EOS) at high density. This EOS is integral to a broad spectrum of disciplines, such as understanding the structure of Jovian planets or designing ignition targets for inertial confinement fusion (ICF).[1,2,3,4] For these reasons, a number of theoretical models of the hydrogen EOS have been proposed.[5–8] The performance of ignition ICF targets on the National Ignition Facility will rely in part on timing the breakout of a sequence of shocks, tuned to minimize the entropy production in the frozen hydrogen (deuterium-tritium) fuel during compression.[9,10] Timing these shocks depends directly on the EOS, again where the molecular fluid transforms to an atomic-partially ionized state.

Hydrogen EOS data at pressures greater than 0.1 Mbar have been obtained by dynamic shock compression and by static compression.[11-15] While both methods can access equilibrium states of matter, the final-state densities and temperatures obtained by shock compression are directly applicable to the Jovian planets and ICF. In shock compression, a single shock drives the fluid to a point on the principal Hugoniot, which is the locus of all final states of pressure, energy and density that are achieved behind a single shock. With the initial state specified, conservation relations require only two independent parameters be measured to obtain an absolute EOS datum. The shock speed, U_s, particle speed U_p, pressure P, internal energy E, and final density ρ are related by:

$$P - P_o = \rho_o U_s U_p \tag{1}$$

$$\rho / \rho_o = U_s / \left(U_s - U_p\right) \tag{2}$$

$$E - E_o = \frac{1}{2}(P + P_o)\left(\frac{1}{\rho_o} - \frac{1}{\rho}\right) \tag{3}$$

where ρ_o is the initial density, P_o is the initial pressure, ρ/ρ_o is the compression, and E_o is the initial internal energy.[16] Equations (1) - (3) are the Hugoniot relations. Notice Hugoniot measurements do not determine temperature, which shows how much internal energy is partitioned into kinetic energy. Temperature is typically determined by measuring the optical emission intensity from the shock front, and must be measured separately.

While early shock wave hydrogen EOS experiments[13] are well described by an intermolecular pair potential model (RRY)[6], recent reshock temperature measurements of Holmes el al. are significantly lower than the RRY model predicts.[14] These lower temperatures are described by a “dissociation model” based on an ideal mixing of molecular states (using a soft-sphere perturbation theory) and monatomic states (using a one-component plasma model). This model contains one adjustable parameter which is set to agree with all the hydrogen shock data,[13,14] and predicts a significantly higher compressibility in the P = 0.2 - 5.0 Mbar regime, than both the RRY model and the Sesame tables.[6,17]

In this paper we describe principle Hugoniot measurements of liquid D_2 up to P = 2.1 Mbar. We compressed liquid D_2 with a Nova-laser-driven shock wave launched from an aluminum pusher. The Al/D_2 interface and the shock front in the D_2 are observed with temporally resolved radiography, to determine U_p, U_S, and ρ/ρ_O. The pressure is calculated using Equation (1). These absolute EOS data reveal a compressibility comparable to the dissociation model.

CRYOGENIC TARGET DESIGN

A schematic of the cryogenic target cell is shown in Fig. 1. Liquid D_2 was contained in a 1-mm-diameter, 0.45-mm-long cylindrical cell machined into a copper block. One end of the cell was sealed with an Al disk that served as the shock pusher; the opposite end of the cell was sealed with a 0.5-mm-thick sapphire window. The pusher was 100, 180, or 250 µm thick, depending on the experiment, and had an rms surface roughness of 30 nm. The pusher was coated with 15 to 25 µm of polystyrene (CH) external to the cell, and the polystyrene was overcoated with a 100 nm layer of Al. The thickness of the polystyrene layer was chosen to prevent direct laser ablation of the Al pusher, to minimize x-ray preheat of the pusher. The Al overcoating eliminated direct laser penetration through the plastic at onset of the laser pulse. To accommodate radiography, a 500-µm-diameter window was drilled into each side of the cell and sealed with a 5-µm-thick beryllium foil. D_2 was loaded into the cell at ~ 20 K and then pressurized to a few hundred torr. Temperatures were monitored to within 0.05 K. Initial D_2 densities were determined from the saturation curve[20] to be 0.171 g/cm^3. The initial density, ρ_O, for each experiment was known to an accracy > 99.5%.

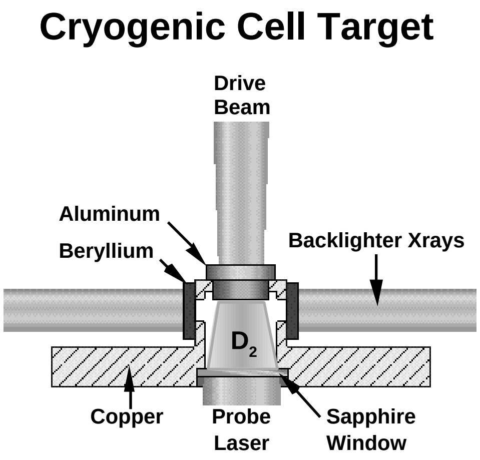

FIGURE 1. Schematic diagram of a cryogenic cell for laser-driven shock compression of liquid deuterium.

EQUATION OF STATE MEASUREMENTS WITH LASERS

It has long been known that lasers are capable of driving very strong shocks into targets.[18] However, laser produced EOS data in the Mbar regiem have been plagued by large errors. There are four issues typically

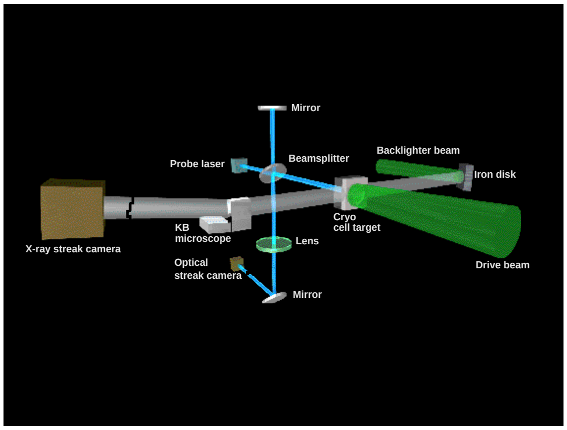

FIGURE 2. Schematic diagram of the experimental setup for simultaneous side-on radiography and end-on interferometry of a cryogenic cell.

preventing accurate laser produced EOS data: shock planarity, preheat, shock steadiness, and measurement accuracy. The experimental layout used for our EOS measurements, which addressed each of the above concerns, is shown in Fig. 2 and described below. First, the shock produced must be planar and spatially uniform. This puts constraints on the target planarity and roughness as well as the drive beam uniformity. One beam of the Nova laser (λ = 527 nm) was focused at normal incidence onto the target, ablating the polystyrene layer and driving a shock wave through the Al and into the D_2. A kinoform phase plate[21] was inserted into the Nova beam to smooth and produce a flat top intensity profile. The laser footprint at the target plane, shown in Fig. 3, was elliptical, with major and minor diameters as great as 900 and 600 µm, respectively, depending on focusing. Lineouts taken through the footprint shows speckle-to-speckle variation ~15% with overall smoothness ~10%.

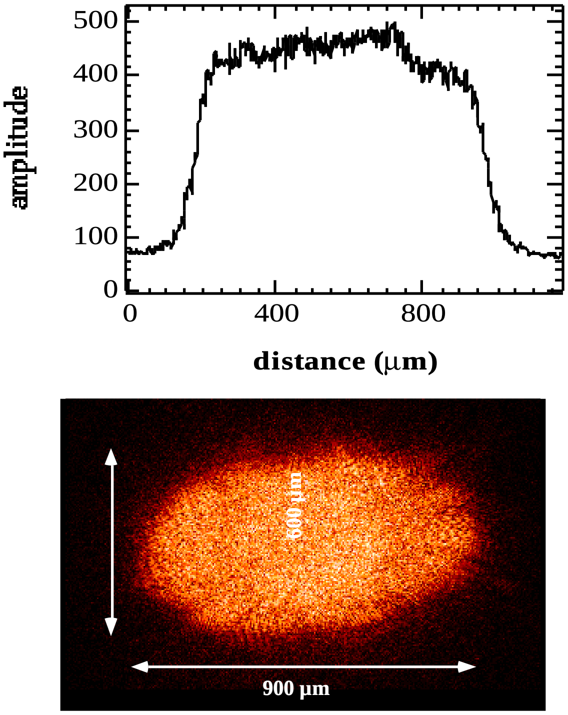

FIGURE 3. Drive laser foot print.

Second, preheat of the sample by penetrating x rays or hot electrons produced in the laser-interaction region must be low. Preheat can cause an uncertainty in the initial state of the sample which translates directly into an uncertainty in the final state. To determine the optimum ablator/pusher combination a series of Lasnex simulations and thermal expansion measurements were performed. A Michelson interferometer, sketched in Fig. 2, measured the thermal expansion of the pusher as well as shock planarity. The Al pusher (at the Al/D_2 interface) forms one arm of a Michelson interferometer. Thus, before shock arrival, if the Aluminum is heated significantly, the sample will begin to expand, causing a shift in the fringe image. Upon shock breakout of the Al, Al unloades into hydrogen, and fringes disappear due to the rapid fringe movement from the large shock velocity. The interferometer-probe beam was a 10-ns-FWHM, 355-nm laser pulse appropriately time-delayed from the Nova drive beam. Results of the calculations and measurements show that a combination of a low Z ablator (~20 µm thick CH) and a thick (100-250 µm depending on drive) Al pusher lowered the preheat of the Al/hydrogen interface to below ~300 C, which is the detection limit of our instrument.

Figure 4 shows the results of 2 different thermal expansion measurements on Al. Figure 4a and 4b show the breakout of aluminum tophat pushers, shown in Fig. 1, during two D_2 EOS experiments. These pushers were 100 µm thick Al with a 1 mm OD and coated with 20 µm of CH and 1000 Å Al. The probe laser beam was reflected off of the rear surface of the Al after passing through a .5 mm thick sapphire window and a .450 mm long reservoir of liquid D_2. The initial cell temperatures were 19.6 K. Figure 4(a) shows the interferogram generated when I ~ 8.5 x 10^{13} W/cm^2. Motion of the D_2/Al pusher interface is clearly observed beginning approximately 4 ns prior to shock breakout. Calculated shock velocities from Lasnex with this ablator/pusher combination scale with intensity, I in W/cm^2,as $Us(\mu m/ns)=24\ (I/10^{14})^{0.287}$, so the predicted breakout occurs at ~ 4.4 ns after the start of the drive beam. Thus preheating is occurring early in the drive pulse. The source of the preheat is likely x rays with energies just under the Al k-edge at 1.56 keV. Since the temperature in the laser deposition region is 1-2 keV, there is a significant x-ray flux at this frequency. Finally, Fig. 4a shows the shock is planar over the central 300-400 µm of the target with rarefaction waves moving inward from the edges causing the observed curvature.

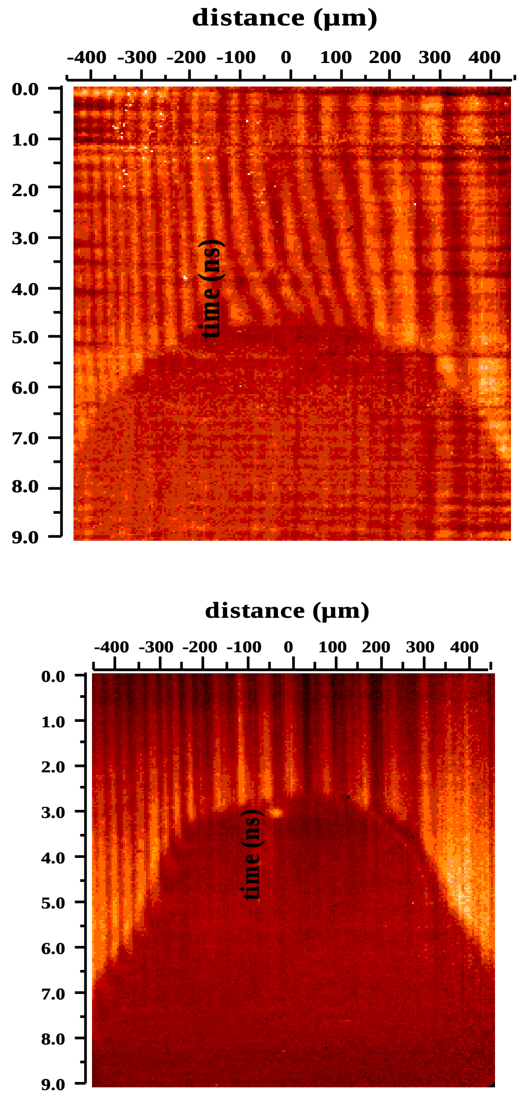

FIGURE 4 streaked fringe images to determine preheat level. Details are discussed in the text

When I is turned down to 1.75 x 10^{13} W/cm^2, no evidence of preheating at the shock front is observed as shown in Figure 4(b). Here the predicted shock breakout time is 6.9 ns after the start of the drive. The region of shock planarity is 200-300 μm. Here, however, a second region of shock curvature is observed. This structure is attributed to the reentrant pusher design. Aluminum plasma moves into the path of the drive beam during its 8 ns duration, effectively reducing the drive laser intensity at the perimeter.

Interferograms of the thicker (180 and 250 μm) pushers exhibited no rear surface motion for I up to 2.4x10^{14} W/cm^2. For a detection limit of 0.2 fringe, which corresponds to movement of 30 nm at the pusher surface, the maximum pusher surface temperature for these targets prior to shock breakout is estimated to be < 400 K.

Finally, shock steadiness and accurate measurements of Us, Up, and ρ/ρ_o were made with high resolution streaked radiography of the shocked hydrogen. Radiography was performed with ~ 800 eV photons from a plasma x-ray source produced by focusing a second beam of Nova onto an Fe disk (10 ns at 6x10^{13} W/cm^2). The backlighter was placed 12 from the target cell to eliminate possible heating of the cell and to produce a near-collimated source. The effective source size in the imaging direction was ~ 150 μm and was set by the width of the laser focal spot. Interferometry shows the x-ray backlighter had no effect on the D_2 in the cell. X rays transmitted through the target cell were imaged by a Kirkpatrick-Baez (K-B) microscope onto a streak camera. The K-B microscope's bandpass was 750-840 eV, and the collection half-angle was 2.5 mrad. Two calibrated magnifications were used: 33× and 82×. The resolution of the K-B microscope in this geometry was found to be better than 3 μm over a 300-μm-wide field of view. The microscope imaged a strip 300 μm long by 5 to 30 μm wide, depending on magnification and configuration. The steak camera was calibrated in space and time by a beat mode radiograph of a gold wire grid. The x-ray pulse train exposure and grid shadow were fit to a series of Gaussians to determine the peaks and thus the absolute time or object position vs. position across the film. The temporal resolution was ~ 20 ps over 8 ns.

A streaked radiograph of shock-compressed D_2 is shown in Fig. 5. I=10^{14} W/cm^2 for 8 ns. The bright area in the figure is the view through the side windows of the cell. Because the pusher is opaque and the liquid transparent, the Al/D_2 interface is the boundary between the light and dark regions. In the figure, the interface is stationary prior to 2 ns. At 2 ns, the laser-driven shock crosses the interface, and the pusher surface accelerates to a steady speed (U_p). The shock front seen moving ahead of the interface is made visible because backlighter x rays grazing the shock-front interface are refracted to greater than 2.5 mrad; out

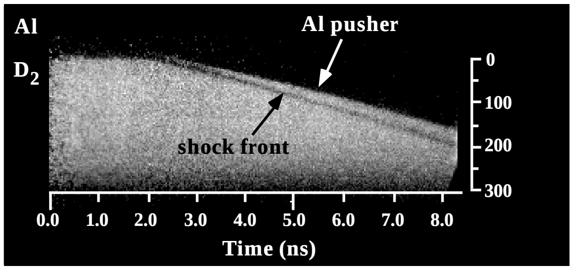

FIGURE 5. A time-resolved, side-on radiograph of laser-shocked D_2. The bright area views the D_2 through beryllium windows bounded by the x-ray-opaque aluminum pusher above. The pusher is seen advancing after breakout at 2 ns; the shock is the dark line in front of and moving faster than the pusher—D_2 interface.

of the angular field of the K-B microscope. Detection of the shock front by refraction is similar to the Schlieren technique for detecting density gradients. The steady propagation of both the shock front and the interface is demonstrated by their linear trajectories until ~ 6 ns, when a stronger shock enters the D_2. First shock U_s and U_p were constant to better than 1%. The second shock is caused by shock reverberations in the pusher. (In this example, no data after 6 ns were used).

U_s and U_p, are evaluated from the slopes, and the single-shock compression can be determined by Eq. (2). Compression can also be measured directly from the film as long as U_s and U_p are constant. At any time t, the compression is equal to the ratio of two lengths: the distance between the shock front $X_2(t)$ and the initial interface position X_o, and the distance between the shock front and the interface $X_1(t)$.

$$\rho / \rho_o = \left(X_2(t) - X_o\right) / \left(X_2(t) - X_1(t)\right).$$

Because all the measurements are made on one piece of film in the streak camera, uncertainties in ρ/ρ_0 due to magnification and sweep speed are canceled. Experiments show a steady U_s and U_p for 4 to 8 ns and values of ρ/ρ_0 calculated directly or using Eq. (2) gave the same results within experimental error.

The shock position observed in the radiograph is the leading part of the shock front that emerged from the center of the pusher. In some experiments, the apparent Al/D_2 interface position at $t = 0$ on film was not identical to the actual value of X_o because the rotation of the cell about the axis perpendicular to both the backlighter path and the shock path could be controlled only to within 3 mrad. This resulted in the center of the pusher being shadowed by an edge of the pusher at very early times. In these cases, X_O was determined by extrapolating the shock and interface position to the point of intersection. This resulted in an increased uncertainty in ρ/ρ_0 from approximately ±3% to approximately ±5%.

The Al/D_2 interface is subject to the Richtmyer-Meshkov hydrodynamic instability (RM). However, using the measured pusher surface finish of 30 nm, we calculated that the largest perturbation expected from RM is less than 0.5 µm during the time of observation.

RESULTS AND CONCLUSION

. Figure 6a shows Us versus Up for our data, the Sesame D_2 EOS table[17], the dissociation model[14], and the D_2 gas gun data[13]. Data above U_s = 20 µm/ns show a significantly different slope as compared to the low pressure data. Figure 6b shows the pressures and final densities determined from the known initial densities and measured compressions. As explained previously, the error bars are governed predominantly by accuracy in determining the slopes of the shock and interface trajectories in the radiographs. The figure also plots the D_2 Hugoniots from the dissociation model,[14] the Sesame D_2 EOS table[17] and the D_2 gas-gun data.[13] At the lowest compression, our data are in agreement with the earlier results; at higher compressions where there is no gas gun data, the laser data show a significantly enhanced compressibility as compared to the Sesame prediction but similar to that of the dissociation model. The Dissociation model shown in Fig. 6 differs slightly from that shown in Ref. 11. The previously reported Hugoniot was a preliminary calculation, and a small conceptual improvement in the theory led to the difference.

In conclusion, these experiments demonstrate that laser-driven shocks can effectively be used for EOS studies at pressures beyond those attainable by traditional techniques. Our results suggest the mass distribution in the Jovian planets is different than previously thought. Also, the more compressible EOS of hydrogen offers higher performance and improved margin for NIF ignition capsules.

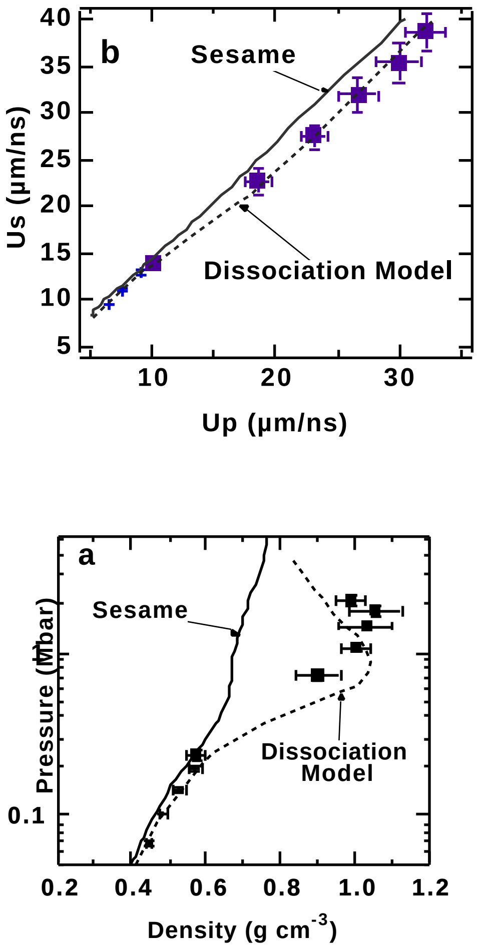

FIGURE 6. D_2 (a) Us versus Up and (b) P versus ρ for our laser produced shock data (dark squares) , gas gun data (dots) Sesame model (solid line), and dissociation model (dashed line).

REFERENCES

1. S. Ichimaru, H. Iyetomi, and S. Tanaka, *Phys. Rep.* **149,** 91 (1987).
2. N. W. Ashcroft, *Phys. World* **8,** (7) 43 (1995).
3. R. Smoluchowski, Nature 215, 691 (1967); V. N. Zharkov and V. P. Trubitsyn, *Jupiter*, T. Gehrels, Ed. (University of Arizona Press, Tucson, 1976) pp. 135-175; W. B. Hubbard, *Science* **214,** 145 (1981); W. J. Nellis, M. Ross, and N. C. Holmes, *Science* **269,** 1249 (1995).
4. J. D. Lindl, *Phys. Plasmas* **2,** 3933 (1995).
5. W. B. Hubbard, *Astrophys. J.* **152,** 745 (1968).
6. M. Ross, F. H. Ree, and D. A. Young, *J. Chem. Phys.* **79,** 1487 (1983).
7. D. Saumon, G. Chabrier, and H. M. Van Horn, *Astrophys. J. Supp.* **99,** 713 (1995).
8. W. R. Magro, D. M. Ceperley, C. Pierleoni, and B. Bernu, *Phys. Rev. Lett.* **76,** 1240 (1996).
9. S. W. Haan, et al., *Phys. Plas.* **2,** 2480 (1995);
10. W. J. Krauser, et al., *Phys. Plas.* **3,** 2084 (1996).
11. L. B. Da Silva, et al., *Phys. Rev. Lett.* (1997).
12. H. K. Mao and R. J. Hemley, *Rev. Mod. Phys.* **66,** 671 (1994).
13. W. J. Nellis, et al., *J. Chem. Phys.* **79,** 1480 (1983).
14. N. C. Holmes, et al., *Phys. Rev. B* **52,** 15835 (1995).
15. S. T. Weir, et al., *Phys. Rev. Lett.* **76,** 1860 (1996).
16. Y. B. Zel'dovich and Y. P. Raizer, *Physics of Shock Waves and High-Temperature Hydrodynamic Phenomena* (Academic Press, New York, 1966).
17. G. I. Kerley, *A Theoretical Equation of State for Deuterium*, Los Alamos Scientific Laboratory Report LA-4776 (New Mexico, January 1972).
18. R. J. Trainor, et al., *Phys. Rev. Lett.* **42,** 1154 (1979).
19. R. Cauble, et al., *Inertial Confinement Fusion, 1993 ICF Annual Report,* UCRL-LR-105820-93, pp. 131-136.
20. P. C. Souers, *Hydrogen Properties for Fusion Energy* (University of California Press, Berkeley, 1986).
21. S. N. Dixit, M. D. Feit, M. D. Perry and H. T. Powell, *Opt. Lett. **21***, 1715 (1996).

*Work performed under the auspices of the U.S. Department of Energy by the Lawrence Livermore National Laboratory under contract number W-7405-ENG-48

Figure 1. Schematic diagram of a cryogenic cell for laser-driven shock compression of liquid deuterium.

Figure 2. Schematic diagram of the experimental setup for simultaneous side-on radiography and end-on interferometry of a cryogenic cell with three laser beams: one smoothed Nova beam to drive a shock in the cell; an oppositely directed Nova beam to provide an x-ray backlighter; and a third (probe) beam for the interferometer.

Figure 3. A time-resolved, side-on radiograph of a laser-shocked D_2 cell. The bright area views the D_2 through beryllium windows bounded by the x-ray-opaque aluminum pusher above. The pusher is seen advancing after breakout at 2 ns; the shock is the dark line in front of and moving faster than the pusher–D_2 interface.

Figure 4. The measured data are shown as squares with error bars compared with Hugoniots derived from the Sesame EOS library,[17] which is similar to an EOS without dissociation,[6] and the proposed dissociation model of Ref. 14. The diamond shapes depict gas-gun data.[13]

Technical Information Department **• Lawrence Livermore National Laboratory**
University of California • Livermore, California 94551